For-Value: Efficient Forward-Only Data Valuation for finetuning LLMs and VLMs

Wenlong Deng[1,2,3,⋆], **Qi Zeng**[3], **Jiaming Zhang**[1], **Minghui Chen**[1], **Zixin Ding**[3], **Christos Thrampoulidis**[1], **Boying Gong**[3†], **Xiaoxiao Li**[1,2†]

[1]University of British Columbia, [2]Vector Institute, [3]Meta

[⋆]Work done at Meta, [†]Corresponding author

Abstract

Data valuation is essential for enhancing the transparency and accountability of large language models (LLMs) and vision-language models (VLMs). However, existing methods typically rely on gradient computations, making them computationally prohibitive for billion-parameter models and precluding batch parallelization. In this work, we introduce `For-Value`, a forward-only data valuation framework that enables efficient batch-scalable value estimation while maintaining effectiveness. Leveraging the expressive power of pretrained LLMs/VLMs, we theoretically demonstrate that data valuation can be captured by the alignment between the final hidden representations and prediction errors at the last layer. In light of this insight, `For-Value` computes data value using a simple closed-form expression with a single forward pass, eliminating the need for costly backpropagation and enabling efficient batch calculating at scale. Extensive experiments show that `For-Value` matches or outperforms gradient-based baselines in detecting influential data and mislabeled data, while achieving significant efficiency improvements. Our code is available at GitHub.

1 Introduction

Modern large language models (LLMs) and vision-language models (VLMs) have achieved remarkable success across a wide range of applications, driven by the power of large-scale pretraining (Achiam et al., 2023). These pretrained models are subsequently fine-tuned for tasks such as machine translation, medical diagnosis, and multimodal reasoning (Guo et al., 2025; Bai et al., 2025b; Wu et al., 2025; Shao et al., 2024; Hao et al., 2025). Despite their impressive performance, these models remain prone to generating factually incorrect or biased outputs (Deng et al., 2023; Ferrara, 2023), often due to the presence of irrelevant, mislabeled, or unrepresentative training data. This highlights the need for scalable methods to quantify the impact of each individual training data and select the high-value samples that benefit the targeted tasks.

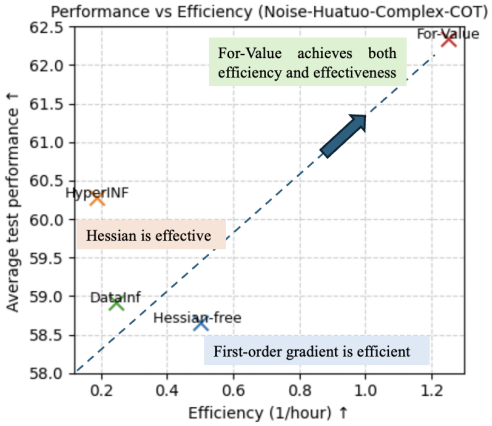

Figure 1: Comparison of data valuation methods in terms of effectiveness and efficiency when selecting training data from the Noise-Huatuo-Complex-CoT dataset for fine-tuning.

The data valuation task aims to assign scores to each training sample based on its effect on model performance on a valuation set (e.g., validation data) (Wang et al., 2025), where performance is commonly assessed using loss, margin, or likelihood (Bae et al., 2024). Notable approaches include influence functions (Kwon et al., 2024) and Shapley value-based methods (Ghorbani and Zou, 2019), which provide frameworks for estimating how individual data points affect model predictions (Kwon et al., 2024; Zhou et al., 2024). These methods have proven effective in downstream applications such as detecting mislabeled data (Koh and Liang, 2017; Kwon et al., 2024), identifying influential examples, diagnosing bias (Kong et al., 2021), and auditing datasets (Grosse et al., 2023). However, these methods are computationally prohibitive for V/LLMs due to reliance on Hessians or repeated retraining.

To mitigate the prohibitive costs of value estimation, prior work has introduced various approxi-

Proceedings of the 64th Annual Meeting of the Association for Computational Linguistics (Volume 1: Long Papers), pages 14581–14600
July 2-7, 2026

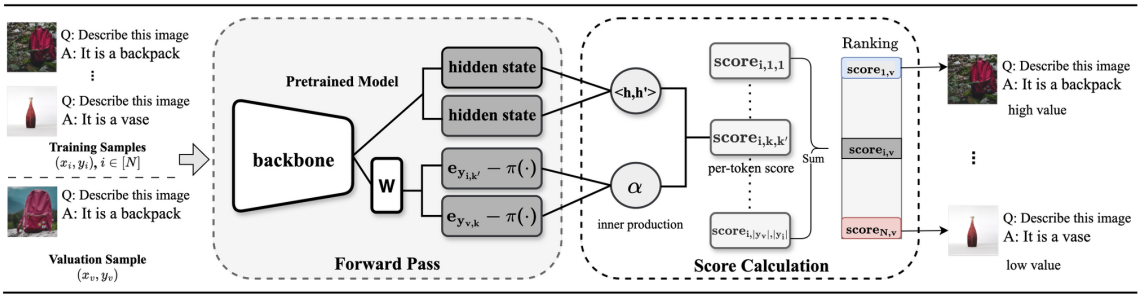

Figure 2: Pipeline of `For-Value`. Given a valuation sample and a training dataset, `For-Value` performs a forward pass over all data to compute scores (Eq. (1)) for each training example, using the last hidden embeddings and the prediction error α. The training samples are then ranked based on these computed values.

mations. TracIn (Pruthi et al., 2020) tracks first-order gradient similarity across checkpoints, while DataInf (Kwon et al., 2024) and HyperInf (Zhou et al., 2024) focus on efficient Hessian approximations. However, these methods incur significant trade-offs, ranging from the massive storage requirements of TracIn to the cubic complexity and scaling errors of Hessian-based approaches, what's more, their reliance on gradient computations necessitates per-sample backpropagation, making it difficult to use large batch sizes for parallel processing. More recently, in run Shapley value (Wang et al., 2025) calculates value along training, but still requires backpropagation and storing per-token gradients and activations, which is costly for long-sequence LLMs; additional multiplications to reconstruct gradients further limit batch scalability. Finally, while training-free similarity metrics exist for other domains (Just et al., 2023; Yang et al., 2025), their foundational assumptions are incompatible with the autoregressive training dynamics of LLMs and VLMs.

In this work, we challenge the necessity of gradient back-propagation for data valuation. Instead, we propose a batch-scalable, forward-only valuation framework by addressing the following core question:

> *Can we achieve scalability via forward-only passes?*

Contributions. We address this foundational question through a rigorous analysis of LLM/VLMs supervised finetuning learning dynamics and extensive empirical evaluation. Our contributions are as follows:

• **Closed-form Data Value Approximation.** We first establish that data value in LLM and VLM fine-tuning can be approximated and derived by *last-layer gradient*. Under the unconstrained feature assumption, we show that the influence of a training sample on a valuation sample, measured via the last-layer gradient, *admits a closed-form expression using only forward inference*: the alignment between their last-layer hidden representations, weighted by similarities in their token-level prediction errors.

• **Scalability via `For-Value`.** By relying only on last-layer hidden representations and token-level prediction errors obtained from a single forward pass, influence scores computed by `For-Value` enable efficient large-batch parallelism and true scalability to modern LLMs and VLMs.

• **Empirical Superiority in Speed and Accuracy.** We conduct extensive experiments on both LLMs and VLMs across a range of downstream tasks (identifying influential & mislabeled samples, and influential data finetuning). `For-Value` achieves both effectiveness and superior efficiency compared to prior data valuation methods.

2 Related Work

Pretrained LLMs and VLMs. Foundation models, such as large language models and vision-language models, serve as powerful initialization points thanks to their extensive pretraining on large-scale datasets. LLMs, including LLaMA (Touvron et al., 2023) and GPT-4 (Achiam et al., 2023), are trained on diverse textual data for language understanding and generation. VLMs, such as Qwen2.5-VL (Bai et al., 2025a), LLaMA-VL (Meta, 2024), and GPT-4V (Yang et al., 2023), integrate visual and textual inputs to perform tasks like image captioning and visual question answering.

Data Valuation. Data valuation aims to measure the contribution of individual training examples in $\mathcal{D}^{\text{train}}$ to a model's performance on a valuation set $\mathcal{D}^{\text{val}}$, typically assessed by loss or likelihood (Bae

et al., 2024; Wang et al., 2025). Most existing approaches are based on influence estimation, ranging from Hessian-based methods (Koh and Liang, 2017) to more scalable approximations such as TracIn (Pruthi et al., 2020), DataInf (Kwon et al., 2024), and HyperInf (Zhou et al., 2024). Despite improved efficiency, these methods still require per-sample gradient computation during or after fine-tuning. Shapley value-based methods (Ghorbani and Zou, 2019) and their online variants (Wang et al., 2025) provide principled alternatives, but remain impractical due to repeated training or the need to compute and store gradients. In contrast to these gradient-dependent approaches, our method enables accurate and batch-scalable data valuation using a single forward pass.

3 Method

In this section, we provide a theoretical justification that the influence of a training sample in LLM and VLM fine-tuning is effectively captured by a closed-form score based on the last-layer gradient. We further show that this score can be effectively computed using `For-Value`, a batch-scalable valuation procedure with forward only.

Notation: Let $\boldsymbol{W}$, $\boldsymbol{w}_z$, and $\boldsymbol{h}_{\boldsymbol{z}}$ denote the token unembedding matrix, unembedding of a token $z \in \mathcal{V}$, where $\mathcal{V}$ is the vocabulary, and hidden embedding of generated tokens $\boldsymbol{z} \in \mathcal{V}^*$ with embedding dimension d, respectively. Let $\boldsymbol{z}_k$ be the k-th token in $\boldsymbol{z}$ and $\boldsymbol{z}_{<k}$ be the first $k-1$ tokens in $\boldsymbol{z}$. Lastly, we denote by $\boldsymbol{e}_z \in \mathbb{R}^{|\mathcal{V}|}$ the standard basis vector corresponding to $z \in \mathcal{V}$.

Formally, given a training dataset $(\boldsymbol{x}_i, \boldsymbol{y}_i)_{i=1}^n \in \mathcal{D}^{\text{train}}$ and a valuation sample $(\boldsymbol{x}_v, \boldsymbol{y}_v) \in \mathcal{D}^{\text{val}}$, we define the notion of *Data Value* as follows:

Definition 1 (Data Value) *At any training time $t > 0$, a training sample is more valuable to a given data point $(\boldsymbol{x}_v, \boldsymbol{y}_v)$ if it results in a greater likelihood change on valuation data $\frac{d}{dt} \ln \pi_{\theta(t)}(\boldsymbol{y}_v|\boldsymbol{x}_v)$.*

This definition captures how much a training sample improves the model's confidence in predicting valuation sample $(\boldsymbol{x}_v, \boldsymbol{y}_v)$. A higher likelihood also corresponds to a lower loss on the valuation data during LLM/VLM fine-tuning. More broadly, our definition of data value is closely tied to the perplexity metric, which inversely reflects the model's uncertainty in text generation. In this work, we focus on the pretrained initialization ($t = 0$) and omit the time index t for brevity.

3.1 Forward-Only Data Value.

Here, we derive the closed-form score from the last-layer gradient. We first state the unconstrained feature assumption:

Assumption 1 (Unconstrained Features) *Expressive (enough) neural networks (e.g., pretrained LLMs/VLMs) can produce unconstrained embeddings $\mathbf{h}_{\boldsymbol{x}} \in \mathbb{R}^d$ independent of the architecture's specific complexities (Mixon et al., 2022; Deng et al., 2025; Zhao et al., 2024). These embeddings are subsequently transformed into logits by a token unembedding matrix $\mathbf{W} \in \mathbb{R}^{|\mathcal{V}|\times d}$. The resulting logits are passed through a softmax function to yield a probability distribution over possible next tokens. To assign probabilities to sequences $\boldsymbol{y} \in \mathcal{V}^*$, the language model π_θ operates in an autoregressive manner, i.e.,*

$$\pi_\theta(\boldsymbol{y} \mid \boldsymbol{x}) = \prod_{k=1}^{|\boldsymbol{y}|} \text{Softmax}(\mathbf{W}\mathbf{h}_{\boldsymbol{x},\boldsymbol{y}_{<k}})_{y_k} .$$

Notably, the unconstrained feature assumption has been widely adopted in the analysis of pretrained LLMs (Mixon et al., 2022; Razin et al., 2024; Zhao et al., 2024). For example, it has been leveraged in reinforcement learning studies (Deng et al., 2025; Razin et al., 2024) and in geometric analyses of LLM representations (Zhao et al., 2024), reinforcing its role as a foundation for `For-Value`. Under the unconstrained feature setting, the influence of a training sample on valuation sample is represented as (detailed proof in Appendix):

Theorem 1 *For a sample $\boldsymbol{x}_v$ and its generation $\boldsymbol{y}_v$ that await valuation, when fine-tuning a pretrained model using a training sample $(\boldsymbol{x}_i, \boldsymbol{y}_i), i \in [n]$, when no training input $\boldsymbol{x}_i$ is identical to the valuation input $\boldsymbol{x}_v$[1], the training data exhibits larger value to the valuation data as the following increases:*

$$\sum_{k=1}^{|\boldsymbol{y}_v|} \sum_{k'=1}^{|\boldsymbol{y}_i|} \alpha_{k,k'} \cdot \left\langle \boldsymbol{h}_{\boldsymbol{x}_v,\boldsymbol{y}_{v,<k}}, \boldsymbol{h}_{\boldsymbol{x}_i,\boldsymbol{y}_{i,<k'}} \right\rangle \quad (1)$$

where $\alpha_{k,k'} = \left\langle \mathbf{e}_{\boldsymbol{y}_{v,k}} - \pi_\theta(\cdot \mid \boldsymbol{x}_v, \boldsymbol{y}_{v,<k}), \mathbf{e}_{\boldsymbol{y}_{i,k'}} - \pi_\theta(\cdot \mid \boldsymbol{x}_i, \boldsymbol{y}_{i,<k'}) \right\rangle$ quantifies the similarity of token-level prediction error across samples.

As stated in the theorem, the data value arises from the alignment between hidden representations and

[1]This assumption is mild, as training inputs often differ from valuation inputs. E.g., in VLMs, images are often unique or paired with different questions. More discussion see Appx.

prediction errors (effect of prediction error see Sec. 5.3). A larger score of Eq. (1) indicates a greater increase in the likelihood of the valuation data. Since Eq. (1) depends on variables resulting from forward, we refer to it as a forward-only data value, termed as `For-Value`.

3.2 Scalable Forward-Only Value Calculation

We now present how to make `For-Value` defined in Eq. (1) scalable. Fig. 2 depicts the overall pipeline, and we detail on each component below.

Sparse Matrix Similarity: We first rewrite Eq. (1) as a matrix inner product. Specifically, by rearranging the computation to perform the summations over k and k' prior to taking the inner product, the overall cost is reduced to that of a single matrix similarity operation. However, directly forming the outer product between the prediction error vector (e.g., $\mathbf{e}_{y_{i,k'}} - \pi_\theta(\cdot \mid \boldsymbol{x}, \boldsymbol{y}_{i,<k'})$) and the hidden embedding incurs a prohibitive computational cost of $O(|\mathcal{V}|\, d)$. To address this, we leverage the sparsity of the predictive distribution: we observe that probability mass is largely concentrated on words appearing in the samples. We therefore restrict the computation to a sample-associated vocabulary $\hat{\mathcal{V}}$. Since $|\hat{\mathcal{V}}| \ll |\mathcal{V}|$, the computational complexity is reduced to $O(|\hat{\mathcal{V}}|\, d)$ (see Tab. 6 for a detailed efficiency analysis). Under this reformulation, the value function admits the following sparse matrix inner product:

$$\left\langle \sum_{k=1}^{|\boldsymbol{y}_v|} \left(\mathbf{e}_{\boldsymbol{y}_{v,k}} - \pi_\theta(\cdot \mid \boldsymbol{x}, \boldsymbol{y}_{v,<k})\right)_{\hat{\mathcal{V}}} \boldsymbol{h}^T_{\boldsymbol{x}_v, \boldsymbol{y}_{v,<k}}, \sum_{k'=1}^{|\boldsymbol{y}_i|} \left(\mathbf{e}_{\boldsymbol{y}_{i,k'}} - \pi_\theta(\cdot \mid \boldsymbol{x}, \boldsymbol{y}_{i,<k'})\right)_{\hat{\mathcal{V}}} \boldsymbol{h}^T_{\boldsymbol{x}_i, \boldsymbol{y}_{i,<k'}} \right\rangle. \tag{2}$$

Moreover, when performing batch valuation, the effective vocabulary can be further restricted to the in-batch vocabulary, as illustrated in Step 6 of Algorithm 1.

`For-Value` Algorithm: Algorithm 1 summarizes the efficient batch computation of `For-Value`. We first obtain hidden embeddings and prediction error vectors for both the valuation and training batches using a single forward pass. We then calculate the score with sparse matrix similarity. Finally, we rank training samples by sorting their resulting influence scores. Importantly, the algorithm can be naturally extended to a group of valuation pairs by averaging their influence scores.

Algorithm 1 For-Value: Forward-Only Data Valuation

Input: Training set $\{(\boldsymbol{x}_i, \boldsymbol{y}_i)\}_{i=1}^N$; valuation pair $(\boldsymbol{x}_v, \boldsymbol{y}_v)$; model π_θ; batch size B.
Output: Data valuation $\mathcal{S}$.

1: Compute $\{\boldsymbol{h}_{\boldsymbol{x}_v, \boldsymbol{y}_{v,<k}}\}_{k=1}^{|\boldsymbol{y}_v|}$ and $\{\pi_\theta(\cdot|\boldsymbol{x}_v, \boldsymbol{y}_{v,<k})\}_{k=1}^{|\boldsymbol{y}_v|}$ by doing inference $\pi_\theta(\boldsymbol{x}_v, \boldsymbol{y}_v)$.
2: **for** each batch $\{(\boldsymbol{x}_j, \boldsymbol{y}_j)\}_{j=1}^B$ **do**
3: Compute $\{\boldsymbol{h}_{\boldsymbol{x}_j, \boldsymbol{y}_{j,<k'}}\}_{k'=1}^{|\boldsymbol{y}_j|}$ and
4: $\{\pi_\theta(\cdot|\boldsymbol{x}_j, \boldsymbol{y}_{j,<k'})\}_{k'=1}^{|\boldsymbol{y}_j|}$ by running batch inference.
5: $\hat{\mathcal{V}} \leftarrow \bigcup_{j=1}^B \mathcal{V}_{\boldsymbol{x}_j, \boldsymbol{y}_j} \cup \mathcal{V}_{\boldsymbol{x}_v, \boldsymbol{y}_v}$
6: Compute errors $(\mathbf{e} - \pi(\cdot))$ for tokens in $\hat{\mathcal{V}}$.
7: For each in batch, compute $S_{v,j}$ via Eq. (2).
8: **end for**
9: $\mathcal{S} \leftarrow \{(\boldsymbol{x}_i, \boldsymbol{y}_i, S_{v,i})\}_{i=1}^N$.
10: Sort $\mathcal{S}$ by $S_{v,i}$ (descending).
11: **return** $\mathcal{S}$.

4 Experiment Setup

In this section, we describe the experimental setup. More details please see Appendix.

Baseline Methods. We focus on the comparison with baseline methods designed for efficiency. Specifically, for parameter-efficiency, we follow `DataInf` (Kwon et al., 2024) and `HyperINF` (Zhou et al., 2024) by applying LoRA modules at each transformer layer. For the hessian efficiency, we use `Hessian-free` (Pruthi et al., 2020; Charpiat et al., 2019) estimates influence scores via the dot product of first-order gradients, which is equivalent to the Trace-Inf (Pruthi et al., 2020) or the first-order in-run Shapley (Wang et al., 2025) at the last training iteration. `DataInf` (Kwon et al., 2024) simplifies the Hessian calculation by swapping the order of the matrix inversion and the average calculations, and `HyperINF` (Zhou et al., 2024) employs a low-rank Fisher approximation of the Hessian. Finally, we include an embedding similarity method (Yang et al., 2025), originally proposed for image generation models, denoted as `Emb`.

Models. Following Kwon et al. (2024), we evaluate LLMs using Llama-2-13B-chat (Touvron et al., 2023) and Qwen-2.5-1.5B (Qwen et al., 2025) to cover a wider range of model sizes and families. Moreover, thanks to the efficiency of our method, we are able to run `For-Value` on Qwen2.5 series models from 7B up to 72B parameters. In contrast, baseline methods require extensive training and

Method	Qwen2.5-1.5B		Llama-2-13B-chat	
	AUC ↑	Recall ↑	AUC ↑	Recall ↑
Sentence transformations				
`Hessian-free`(Pruthi et al., 2020)	0.785 ± 0.096	0.370 ± 0.139	0.999 ± 0.002	0.985 ± 0.033
`DataInf`(Kwon et al., 2024)	0.981 ± 0.019	0.826 ± 0.121	$\mathbf{1.000 \pm 0.000}$	0.997 ± 0.010
`HyperINF`(Zhou et al., 2024)	0.993 ± 0.013	0.934 ± 0.063	$\mathbf{1.000 \pm 0.000}$	0.998 ± 0.011
`Emb`(Yang et al., 2025)	0.546 ± 0.306	0.148 ± 0.205	0.854 ± 0.192	0.563 ± 0.412
`For-Value` (ours)	$\mathbf{1.000 \pm 0.001}$	$\mathbf{0.989 \pm 0.025}$	$\mathbf{1.000 \pm 0.000}$	$\mathbf{1.000 \pm 0.001}$
Math Problem (w/o reasoning)				
`Hessian-free`(Pruthi et al., 2020)	0.835 ± 0.235	0.592 ± 0.291	0.770 ± 0.174	0.258 ± 0.388
`DataInf`(Kwon et al., 2024)	0.985 ± 0.032	0.878 ± 0.154	$\mathbf{1.000 \pm 0.000}$	0.999 ± 0.006
`HyperINF`(Zhou et al., 2024)	0.986 ± 0.024	0.942 ± 0.080	0.995 ± 0.018	0.967 ± 0.057
`Emb`(Yang et al., 2025)	0.555 ± 0.298	0.146 ± 0.295	0.762 ± 0.239	0.389 ± 0.477
`For-Value` (ours)	$\mathbf{1.000 \pm 0.000}$	$\mathbf{0.998 \pm 0.011}$	$\mathbf{1.000 \pm 0.000}$	$\mathbf{1.000 \pm 0.002}$ [2]
Math Problem (w/ reasoning)				
`Hessian-free`(Pruthi et al., 2020)	0.829 ± 0.172	0.524 ± 0.350	0.772 ± 0.173	0.258 ± 0.388
`DataInf`(Kwon et al., 2024)	0.987 ± 0.030	0.892 ± 0.155	1.000 ± 0.001	0.996 ± 0.025
`HyperINF`(Zhou et al., 2024)	0.988 ± 0.023	0.950 ± 0.060	0.994 ± 0.018	0.961 ± 0.074
`Emb`(Yang et al., 2025)	0.560 ± 0.310	0.198 ± 0.311	0.725 ± 0.217	0.270 ± 0.420
`For-Value` (ours)	$\mathbf{1.000 \pm 0.000}$	$\mathbf{0.998 \pm 0.008}$	$\mathbf{1.000 \pm 0.000}$	$\mathbf{1.000 \pm 0.000}$

Table 1: Influential data identification results on LLMs. `For-Value` consistently achieves comparable or superior performance. Results are reported as Mean ± Standard Deviation (std).

prolonged runtimes, making them costly for these larger models. For VLMs, we adopt the widely used Qwen-2.5-VL-3B-Instruct (Bai et al., 2025a) and Llama-3.2-11B-Vision (Meta, 2024).

Influential Data Identification. We evaluate all methods on influential data identification for LLMs and VLMs, following Kwon et al. (2024). For LLMs, we use sentence transformation and math word problem datasets (w and w/o reasoning). For VLMs, we adapt image-to-text tasks from Kwon et al. (2024) to an image-to-text generation setting, including style generation (cartoons, pixel art, line sketches) and subject generation using the DreamBooth dataset (Ruiz et al., 2023). We adopt two evaluation metrics from Kwon et al. (2024): (i) AUC, measuring the correlation between data values and pseudo-labels (1 if training and valuation samples share a class, 0 otherwise), averaged over valuation points; and (ii) Recall, the proportion of top-ranked training samples sharing the same class as the valuation point. More details and dataset examples see Appendix Sec. A.5.

Mislabeled Data Detection. We evaluate mislabeled data detection on VLMs using the Kaggle cat–dog dataset (kag, 2013), reformulated as a QA task with 50% label being flipped, and report AUC and Recall; examples and further details are provided in the Appendix Sec. A.5.

Data Selection For Finetuning. We evaluate the practical utility of `For-Value` across two key reasoning domains: mathematics and medicine. For mathematics, we use the GSM8K (Cobbe et al., 2021) dataset to assess influential data identification, while for medicine, we employ the Noise-Huatuo-Complex-CoT (Chen et al., 2024) dataset to examine robustness under noisy training. We further extend our study to vision–language models by applying `For-Value` to PMC-Reasoning (Huang et al., 2025). More details for each task are provided in Appendix Sec. A.3.

Efficiency Evaluation. For influential and mislabeled data detection with models under 32B, we compute data values using a single A100 (80G) GPU with identical hardware settings. For finetuning data selection, we use a single H100 (96G) GPU to calculate the data value for fair comparison. More details please see Appendix Sec. A.1.

5 Results

In this section, we detail the results of `For-Value` and baselines on LLMs and VLMs.

5.1 Identify Influential & Mislabeled Data

Influential data identification Results on LLM. We first present the results for text generation tasks in Tab. 1, where `For-Value` consistently matches or outperforms all baseline methods across the evaluated LLM benchmarks:

(1) *Sentence Transformation:* As shown in Tab. 1, `For-Value` achieves perfect or near-perfect AUC

Method	Qwen2.5-VL-3B-Instruct		Llama-3.2-11B-vision	
	AUC ↑	Recall ↑	AUC ↑	Recall ↑
Image-to-text subject generation				
Hessian-free(Pruthi et al., 2020)	0.979 ± 0.038	0.738 ± 0.399	0.961 ± 0.093	0.765 ± 0.365
DataInf(Kwon et al., 2024)	0.989 ± 0.024	0.836 ± 0.318	0.958 ± 0.119	0.797 ± 0.323
HyperINF(Zhou et al., 2024)	0.988 ± 0.047	$\mathbf{0.902 \pm 0.220}$	0.993 ± 0.025	0.919 ± 0.186
Emb(Yang et al., 2025)	0.841 ± 0.189	0.206 ± 0.458	0.841 ± 0.189	0.206 ± 0.379
For-Value (ours)	$\mathbf{0.994 \pm 0.018}$	0.897 ± 0.287	$\mathbf{0.995 \pm 0.040}$	$\mathbf{0.985 \pm 0.068}$
Image-to-text style generation				
Hessian-free(Pruthi et al., 2020)	0.515 ± 0.096	0.799 ± 0.162	0.515 ± 0.079	0.824 ± 0.145
DataInf(Kwon et al., 2024)	0.520 ± 0.094	0.760 ± 0.181	0.515 ± 0.174	0.785 ± 0.164
HyperINF(Zhou et al., 2024)	0.516 ± 0.055	0.860 ± 0.103	0.490 ± 0.090	0.821 ± 0.137
Emb(Yang et al., 2025)	0.560 ± 0.310	0.198 ± 0.311	0.553 ± 0.294	0.340 ± 0.467
For-Value (ours)	$\mathbf{0.895 \pm 0.138}$	$\mathbf{0.916 \pm 0.153}$	$\mathbf{0.974 \pm 0.059}$	$\mathbf{0.997 \pm 0.013}$
Mislabeled Data Detection				
Hessian-free(Pruthi et al., 2020)	0.719 ± 0.098	0.760 ± 0.088	0.962 ± 0.019	0.955 ± 0.068
DataInf(Kwon et al., 2024)	0.760 ± 0.088	0.901 ± 0.147	$\mathbf{1.000 \pm 0.000}$	1.000 ± 0.003
HyperINF(Zhou et al., 2024)	0.770 ± 0.077	0.916 ± 0.128	1.000 ± 0.001	1.000 ± 0.006
Emb(Yang et al., 2025)	0.741 ± 0.061	0.533 ± 0.075	0.933 ± 0.044	0.996 ± 0.015
For-Value (ours)	$\mathbf{0.885 \pm 0.055}$	$\mathbf{0.999 \pm 0.010}$	0.995 ± 0.008	$\mathbf{1.000 \pm 0.000}$

Table 2: Influential data identification and mislabeled data detection performance for different VLM tasks. For-Value consistently delivers comparable or superior performance in identifying influential data and detecting mislabeled data across various VLM tasks compared to baseline methods.

and recall scores for both models. Notably, on Qwen2.5-1.5B, For-Value surpasses the strongest baseline HyperINF by 6.5% in recall.

(2) *Math Problems (w/&w/o reasoning):* A similar pattern holds for the math task. As shown in Tab. 1, For-Value delivers higher-quality influence identification with just a single forward pass, improving recall by 6% over HyperINF on both math datasets with the Qwen model.

Influential data identification Results on VLM. We next report the results on VLMs in Tab. 2. (1) For subject generation, For-Value achieves the highest AUC and recall scores for both models, consistently outperforming all baselines. Specifically, For-Value exceeds the strongest baseline, HyperINF, by more than 7% in recall for both models for the 11B model. (2) In the more challenging style generation task, For-Value demonstrates a clear advantage, with AUC improvements of over 0.35 compared to the baselines, and even larger gains over the Emb method.

Mislabeled Data Detection. Our mislabeled data detection results in Tab. 2 demonstrate For-Value's strong performance across model scales. On the Qwen-VL-3B model, For-Value achieves an 11.5% higher AUC and an 8.3% higher Recall compared to the best baseline (HyperINF), showing significant improvements in identifying mislabeled examples. The method performs equally well on the larger Llama-3.2-11B model, matching the near-perfect detection rates (AUC $>$ 0.99, Recall = 1.0) of gradient-based approaches. This consistent performance across both models highlights For-Value's effectiveness. Additional results of For-Value under varying noise ratios are reported in Tab. 7.

[2]AUC and Recall values reported as 1.0 may still include a non-zero std due to rounding. The large std arises since value distribution is highly polarized, clustering near either 1 or 0.

Llama-3.1-8B	GSM8K (1%) ↑	GSM8K (5%) ↑	Time ↓
Full (100%)	47.8		–
Hessian-free	41.5	41.8	1.4 h
HyperINF	41.9	42.8	2.4 h
DataInf	41.7	42.0	1.9 h
For-Value (ours)	**45.2**	**48.3**	**0.3 h**

Table 3: GSM8K greedy decoding accuracy of Llama-3.1-8B. Best results are in **bold**.

5.2 Data Selection For Finetuning

We next assess For-Value's practical utility on mathematics and medicine. Given poor performance of Emb in prior experiments, we excluded it from these evaluations.

Mathematics: GSM8K. We evaluate influential data identification on GSM8K (Cobbe et al., 2021) using test reasoning examples as valuation data, where high-value training samples are expected to improve test accuracy. Following (Deng

Method (Llama-3.1-8B-Ins)	MedQA	MedMCQA	PubMedQA	MMLU-Pro-med	GPQA-med	Average ↑	Time ↓
Base	56.84	61.90	77.00	59.02	44.35	59.82	–
5% Data							
`Hessian-free`	55.41	58.05	73.40	54.53	38.46	55.97	2.0 (h)
`HyperINF`	55.15	57.58	71.50	54.14	43.08	56.29	5.3 (h)
`DataInf`	55.39	57.74	73.30	54.07	45.13	57.13	4.1 (h)
`For-Value` (ours)	**56.80**	**62.92**	**77.60**	**58.31**	**45.90**	**60.31**	**0.8 (h)**
10% Data							
`Hessian-free`	57.02	59.15	72.30	57.13	47.69	58.66	2.0 (h)
`HyperINF`	56.94	62.76	77.40	57.85	48.46	60.28	5.3 (h)
`DataInf`	56.61	61.74	75.60	56.81	43.85	58.92	4.1 (h)
`For-Value` (ours)	**57.61**	**67.16**	**78.30**	**58.18**	**50.51**	**62.35**	**0.8 (h)**

Table 4: Results of data selection for fine-tuning on the Noise Huatuo-Complex-CoT (Llama-3.1-8B-Ins).

Method (Qwen2.5-VL-3B)	MMMU	MedX-M	PathVQA	PMC	SLAKE	VQA-Rad	Average ↑	Time ↓
Base	44.12	20.69	61.96	44.77	61.30	62.01	49.14	–
Full* (Huang et al., 2025)	47.84	21.46	52.76	54.55	65.79	58.58	50.16	–
10% Data								
`Hessian-free`	48.82	20.65	61.18	49.60	61.78	63.60	50.94	1.3 (h)
`HyperINF`	**50.00**	21.60	61.10	50.45	62.50	63.97	<u>51.60</u>	1.7 (h)
`DataInf`	49.41	21.10	62.64	**50.55**	59.38	**65.81**	51.48	1.6 (h)
`For-Value` (ours)	47.06	**23.05**	**62.93**	49.55	**67.55**	63.24	**52.23**	**0.4 (h)**
20% Data								
`Hessian-free`	52.94	21.40	61.81	52.05	63.46	62.50	52.36	1.3 (h)
`HyperINF`	**56.47**	20.50	**62.14**	**51.45**	62.98	**64.71**	**53.04**	1.7 (h)
`DataInf`	48.82	21.25	62.58	51.35	63.46	63.24	51.78	1.6 (h)
`For-Value` (ours)	54.12	**22.45**	60.26	50.45	**65.14**	63.60	<u>52.67</u>	**0.4 (h)**

Table 5: Results of data selection for fine-tuning on the PMC-Reasoning dataset. Best results are in **bold**, and second-best are <u>underlined</u>. * denotes results from (Huang et al., 2025).

et al., 2024), we report greedy fine-tuning results in Tab. 3. Fine-tuning on the top 5% samples selected by `For-Value` achieves the highest accuracy of 48.3%, surpassing the strongest baseline, `HyperINF`, by 5.5%, and slightly outperforming training on the full dataset, as expected when using test data for valuation. Reducing the selection rate to 1% lowers performance, but `For-Value` still exceeds all baselines by up to 3.3%. Importantly, `For-Value` is over $5\times$ faster than all baselines.

Medicine: Noise-Huatuo-Complex-CoT. To examine robustness under noisy training conditions, we construct a corrupted version of the Huatuo-Complex-CoT dataset (Chen et al., 2024). We randomly sample 5,000 examples without replacement and inject noise into 40% of them by inserting or removing irrelevant words (Wei and Zou, 2019) (examples see Fig. 7 in Appendix), resulting in the Noise-Huatuo-Complex-CoT dataset. Another 5,000 clean examples are reserved for valuation, and models are evaluated on five held-out medical QA test sets. Within this setting, we apply `For-Value` and competing methods to select high-quality training subsets for fine-tuning. As shown in Tab. 4, `For-Value` consistently delivers the strongest results. With only 5% data, it reaches an average accuracy of 60.31%, outperforming the best baseline (`DataInf`) by 3%. At 10%, `For-Value` shows an even clearer advantage, achieving the best score across all tasks with an average of 62.35%, exceeding the strongest baseline `HyperINF` by 2.1%. Crucially, `For-Value` also provides the most efficient valuation, requiring only 0.8h, up to $6\times$ faster than baselines. These results underscore the effectiveness of `For-Value` in identifying valuable data even when training data is noisy. More analysis see Appendix Sec. A.4.

Medical VQA. To evaluate the effectiveness of `For-Value` on vision–language models, we conduct experiments on the PMC-Reasoning dataset (Zhang et al., 2023). We randomly sample 10,000 examples for training and 5,000 for valuation without replacement. Fine-tuning subsets are then selected from the training pool using `For-Value` as well as baseline methods, and the resulting models are fine-tuned and evaluated on six held-out test sets. As shown in Tab. 5, `For-Value` delivers the strongest overall performance. With 10% data, it achieves the highest average accuracy (52.23%), exceeding the base model by over 3% and the best-performing baseline, `HyperINF`, by 0.6%. At 20% data, `For-Value` maintains compet-

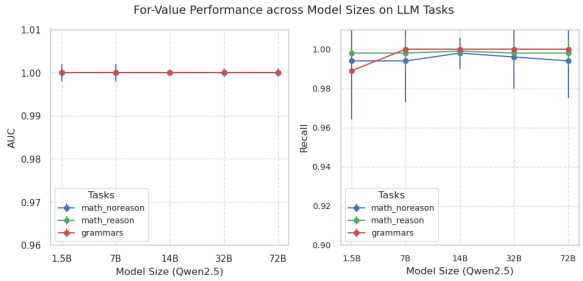

Figure 3: `For-Value` performance across model sizes and tasks (Mean±std).

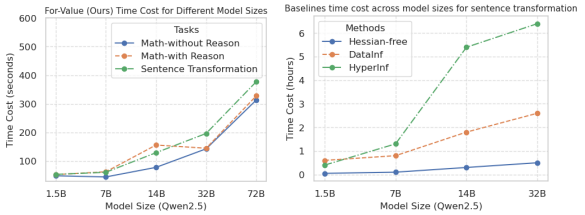

(a) `For-Value`. (b) Baseline Methods

Figure 4: Time cost analysis: (a) `For-Value` across different model sizes and tasks. (b) Baseline methods on the sentence transformation task across model sizes. `For-Value` is more efficient with time costs measured in seconds, whereas baselines require up to several hours.

itive performance (52.67%), ranking second only to `HyperINF`. Importantly, `For-Value` consistently achieves these results with the lowest computational cost (0.4h vs. 1.6–1.7h for baseline methods). Notably, all data valuation methods surpass full fine-tuning, highlighting the benefit of selecting high-value subsets for training. Overall, `For-Value` reliably identifies influential medical VQA data while offering large efficiency gains.

5.3 Ablation Study & Efficiency

We present ablation and efficiency studies based on influential and mislabeled data identification tasks.

Effect of prediction error similarity α. We perform an ablation study to evaluate the role of the α term by setting α to 1 in the computation of Eq. (2). This simplification reduces the score to $\left\langle \sum_{k=1}^{|\boldsymbol{y}_v|} \boldsymbol{h}_{\boldsymbol{x}_v,\boldsymbol{y}_{v,<k}}, \sum_{k'=1}^{|\boldsymbol{y}_i|} \boldsymbol{h}_{\boldsymbol{x}_i,\boldsymbol{y}_{i,<k'}} \right\rangle$, which measures contextualized text embedding similarity between two data samples' $\boldsymbol{y}$ and is equivalent to the `Emb` baseline. As shown in Tab. 1 and 2, `For-Value` consistently outperforms `Emb` across both LLM and VLM tasks, highlighting the importance of the α term. The prediction error in α acts as a token-level weight, down-weighting tokens that are already confidently predicted in either the training or valuation data. While `Emb` is effective for generative image models, its degraded performance indicates that directly applying embedding similarity to LLMs/VLMs is suboptimal due to differing training objectives.

`For-Value` Performance across model sizes. Fig. 3 shows that `For-Value` maintains consistently high performance across different model sizes and tasks. Both AUC and Recall stay close to 1.0 for all tasks, indicating that scaling up the model does not degrade effectiveness. This stability confirms that `For-Value` generalizes well to larger models while preserving accuracy, making it reliable for practical deployment on LLM tasks.

Effectiveness of last-layer gradient. The Hessian-free baseline follows the setup of DataInf (Kwon et al., 2024), computing gradient similarity over LoRA parameters across all transformer layers. In contrast, `For-Value` relies solely on the last-layer gradient. As shown in Tab. 1 to 4, `For-Value` consistently matches or outperforms `Hessian-free`, demonstrating that the last-layer gradient provides an effective measure of data value and further supporting our theoretical analysis in Theorem 1.

Time Cost Analysis. We compare the time cost of `For-Value` with that of the baselines across model sizes using influential data identification tasks on a single GPU. As shown in Fig. 4a, `For-Value` maintains consistently low runtime, even as model size increases from 1.5B to 72B parameters. For all tasks, the runtime remains within a few hundred seconds, highlighting its practical scalability. In contrast, as shown in Fig. 4b, baseline methods for the sentence transformation task require more time—measured in hours rather than seconds. The best-performing baseline, `HyperINF`, becomes costly for larger models, taking 6 hours for the 32B model. This underscores the efficiency advantage of `For-Value`. More details see Sec. A.2.

6 Conclusion

We theoretically show that data influence can be accurately approximated by the alignment between last-layer hidden representations and token-level prediction errors, eliminating the need for backpropagation. Building on this insight, we introduce `For-Value`, a forward-only data valuation framework for pretrained LLMs and VLMs. Using a single forward pass, `For-Value` matches existing methods in identifying influential and mislabeled data and in selecting high-value subsets for fine-tuning, while being substantially more efficient.

7 Limitations

Our method is tailored to data valuation in the fine-tuning stage and is not directly applicable to pre-training data selection, where the unconstrained feature assumption may not hold. Nevertheless, fine-tuning remains a critical stage for adapting pretrained models to downstream tasks. In addition, data value may evolve over the course of training. Extending `For-Value` to support stage-aware data selection or active learning is left for future work, though we believe such extensions can be incorporated naturally.

8 Acknowledgments

The research is supported, in part, by the NSERC; NSERC Discovery Grant RGPIN-2022-05316, RGPIN-2021-03677; NSERC Alliance Grant ALLRP 602633-24, 581098-22; Tri-Agency Canada; Canada CIFAR AI Chair Awards; Canada Research Chair Fellowship; IITP grant; the Ministry of Science and ICT (RS-2024-00445087, RS2025-25464461).

References

2013. Dogs vs. cats dataset. https://www.kaggle.com/c/dogs-vs-cats. Accessed: 2023-10-18.

Josh Achiam, Steven Adler, Sandhini Agarwal, Lama Ahmad, Ilge Akkaya, Florencia Leoni Aleman, Diogo Almeida, Janko Altenschmidt, Sam Altman, Shyamal Anadkat, and 1 others. 2023. Gpt-4 technical report. *arXiv preprint arXiv:2303.08774*.

Juhan Bae, Wu Lin, Jonathan Lorraine, and Roger B Grosse. 2024. Training data attribution via approximate unrolling. *Advances in Neural Information Processing Systems*, 37:66647–66686.

Shuai Bai, Keqin Chen, Xuejing Liu, Jialin Wang, Wenbin Ge, Sibo Song, Kai Dang, Peng Wang, Shijie Wang, Jun Tang, Humen Zhong, Yuanzhi Zhu, Mingkun Yang, Zhaohai Li, Jianqiang Wan, Pengfei Wang, Wei Ding, Zheren Fu, Yiheng Xu, and 8 others. 2025a. Qwen2.5-vl technical report. *Preprint*, arXiv:2502.13923.

Shuai Bai, Keqin Chen, Xuejing Liu, Jialin Wang, Wenbin Ge, Sibo Song, Kai Dang, Peng Wang, Shijie Wang, Jun Tang, and 1 others. 2025b. Qwen2. 5-vl technical report. *arXiv preprint arXiv:2502.13923*.

Guillaume Charpiat, Nicolas Girard, Loris Felardos, and Yuliya Tarabalka. 2019. Input similarity from the neural network perspective. *Advances in Neural Information Processing Systems*, 32.

Junying Chen, Zhenyang Cai, Ke Ji, Xidong Wang, Wanlong Liu, Rongsheng Wang, Jianye Hou, and Benyou Wang. 2024. Huatuogpt-o1, towards medical complex reasoning with llms. *arXiv preprint arXiv:2412.18925*.

Pinaki Nath Chowdhury, Aneeshan Sain, Ayan Kumar Bhunia, Tao Xiang, Yulia Gryaditskaya, and Yi-Zhe Song. 2022. Fs-coco: Towards understanding of freehand sketches of common objects in context. In *ECCV*.

Karl Cobbe, Vineet Kosaraju, Mohammad Bavarian, Mark Chen, Heewoo Jun, Lukasz Kaiser, Matthias Plappert, Jerry Tworek, Jacob Hilton, Reiichiro Nakano, and 1 others. 2021. Training verifiers to solve math word problems. *arXiv preprint arXiv:2110.14168*.

Wenlong Deng, Yi Ren, Muchen Li, Danica J Sutherland, Xiaoxiao Li, and Christos Thrampoulidis. 2025. On the effect of negative gradient in group relative deep reinforcement optimization. *arXiv preprint arXiv:2505.18830*.

Wenlong Deng, Yize Zhao, Vala Vakilian, Minghui Chen, Xiaoxiao Li, and Christos Thrampoulidis. 2024. Dare the extreme: Revisiting delta-parameter pruning for fine-tuned models. *arXiv preprint arXiv:2410.09344*.

Wenlong Deng, Yuan Zhong, Qi Dou, and Xiaoxiao Li. 2023. On fairness of medical image classification with multiple sensitive attributes via learning orthogonal representations. In *International Conference on Information Processing in Medical Imaging*, pages 158–169. Springer.

Emilio Ferrara. 2023. Should chatgpt be biased? challenges and risks of bias in large language models. *arXiv preprint arXiv:2304.03738*.

Amirata Ghorbani and James Zou. 2019. Data shapley: Equitable valuation of data for machine learning. In *International conference on machine learning*, pages 2242–2251. PMLR.

Roger Grosse, Juhan Bae, Cem Anil, Nelson Elhage, Alex Tamkin, Amirhossein Tajdini, Benoit Steiner, Dustin Li, Esin Durmus, Ethan Perez, and 1 others. 2023. Studying large language model generalization with influence functions. *arXiv preprint arXiv:2308.03296*.

Daya Guo, Dejian Yang, Haowei Zhang, Junxiao Song, Ruoyu Zhang, Runxin Xu, Qihao Zhu, Shirong Ma, Peiyi Wang, Xiao Bi, and 1 others. 2025. Deepseek-r1: Incentivizing reasoning capability in llms via reinforcement learning. *arXiv preprint arXiv:2501.12948*.

Yunzhuo Hao, Jiawei Gu, Huichen Will Wang, Linjie Li, Zhengyuan Yang, Lijuan Wang, and Yu Cheng. 2025. Can mllms reason in multimodality? emma: An enhanced multimodal reasoning benchmark. *arXiv preprint arXiv:2501.05444*.

Xuehai He, Yichen Zhang, Luntian Mou, Eric Xing, and Pengtao Xie. 2020. Pathvqa: 30000+ questions for medical visual question answering. *arXiv preprint arXiv:2003.10286*.

Xiaoke Huang, Juncheng Wu, Hui Liu, Xianfeng Tang, and Yuyin Zhou. 2025. Medvlthinker: Simple baselines for multimodal medical reasoning. *arXiv preprint arXiv:2508.02669*.

Jainr3. 2023. jainr3/diffusiondb-pixelart · Datasets at Hugging Face. https://huggingface.co/datasets/jainr3/diffusiondb-pixelart. [Accessed 24-09-2023].

Di Jin, Eileen Pan, Nassim Oufattole, Wei-Hung Weng, Hanyi Fang, and Peter Szolovits. 2021. What disease does this patient have? a large-scale open domain question answering dataset from medical exams. *Applied Sciences*, 11(14):6421.

Qiao Jin, Bhuwan Dhingra, Zhengping Liu, William W Cohen, and Xinghua Lu. 2019. Pubmedqa: A dataset for biomedical research question answering. *arXiv preprint arXiv:1909.06146*.

Hoang Anh Just, Feiyang Kang, Jiachen T Wang, Yi Zeng, Myeongseob Ko, Ming Jin, and Ruoxi Jia. 2023. Lava: Data valuation without pre-specified learning algorithms. *arXiv preprint arXiv:2305.00054*.

Pang Wei Koh and Percy Liang. 2017. Understanding black-box predictions via influence functions. In *International conference on machine learning*, pages 1885–1894. PMLR.

Shuming Kong, Yanyan Shen, and Linpeng Huang. 2021. Resolving training biases via influence-based data relabeling. In *International Conference on Learning Representations*.

Yongchan Kwon, Eric Wu, Kevin Wu, and James Zou. 2024. Datainf: Efficiently estimating data influence in lora-tuned llms and diffusion models. *International Conference on Learning Representations*.

Jason J Lau, Soumya Gayen, Asma Ben Abacha, and Dina Demner-Fushman. 2018. A dataset of clinically generated visual questions and answers about radiology images. *Scientific data*, 5(1):1–10.

Bo Liu, Li-Ming Zhan, Li Xu, Lin Ma, Yan Yang, and Xiao-Ming Wu. 2021. Slake: A semantically-labeled knowledge-enhanced dataset for medical visual question answering. In *2021 IEEE 18th international symposium on biomedical imaging (ISBI)*, pages 1650–1654. IEEE.

AI Meta. 2024. Llama 3.2: Revolutionizing edge ai and vision with open, customizable models. *Meta AI Blog. Retrieved December*, 20:2024.

Dustin G Mixon, Hans Parshall, and Jianzong Pi. 2022. Neural collapse with unconstrained features. *Sampling Theory, Signal Processing, and Data Analysis*, 20(2):11.

Norod78. 2023. Norod78/cartoon-blip-captions · Datasets at Hugging Face. https://huggingface.co/datasets/Norod78/cartoon-blip-captions. [Accessed 24-09-2023].

Ankit Pal, Logesh Kumar Umapathi, and Malaikannan Sankarasubbu. 2022. Medmcqa: A large-scale multi-subject multi-choice dataset for medical domain question answering. In *Conference on health, inference, and learning*, pages 248–260. PMLR.

Garima Pruthi, Frederick Liu, Satyen Kale, and Mukund Sundararajan. 2020. Estimating training data influence by tracing gradient descent. *Advances in Neural Information Processing Systems*, 33:19920–19930.

Qwen, :, An Yang, Baosong Yang, Beichen Zhang, Binyuan Hui, Bo Zheng, Bowen Yu, Chengyuan Li, Dayiheng Liu, Fei Huang, Haoran Wei, Huan Lin, Jian Yang, Jianhong Tu, Jianwei Zhang, Jianxin Yang, Jiaxi Yang, Jingren Zhou, and 25 others. 2025. Qwen2.5 technical report. *Preprint*, arXiv:2412.15115.

Noam Razin, Sadhika Malladi, Adithya Bhaskar, Danqi Chen, Sanjeev Arora, and Boris Hanin. 2024. Unintentional unalignment: Likelihood displacement in direct preference optimization. *arXiv preprint arXiv:2410.08847*.

David Rein, Betty Li Hou, Asa Cooper Stickland, Jackson Petty, Richard Yuanzhe Pang, Julien Dirani, Julian Michael, and Samuel R Bowman. 2024. Gpqa: A graduate-level google-proof q&a benchmark. In *First Conference on Language Modeling*.

Nataniel Ruiz, Yuanzhen Li, Varun Jampani, Yael Pritch, Michael Rubinstein, and Kfir Aberman. 2023. Dreambooth: Fine tuning text-to-image diffusion models for subject-driven generation. In *Proceedings of the IEEE/CVF conference on computer vision and pattern recognition*, pages 22500–22510.

Zhihong Shao, Peiyi Wang, Qihao Zhu, Runxin Xu, Junxiao Song, Xiao Bi, Haowei Zhang, Mingchuan Zhang, YK Li, Y Wu, and 1 others. 2024. Deepseekmath: Pushing the limits of mathematical reasoning in open language models. *arXiv preprint arXiv:2402.03300*.

Hugo Touvron, Louis Martin, Kevin Stone, Peter Albert, Amjad Almahairi, Yasmine Babaei, Nikolay Bashlykov, Soumya Batra, Prajjwal Bhargava, Shruti Bhosale, and 1 others. 2023. Llama 2: Open foundation and fine-tuned chat models. *arXiv preprint arXiv:2307.09288*.

Jiachen T Wang, Prateek Mittal, Dawn Song, and Ruoxi Jia. 2025. Data shapley in one training run. *International conference on machine learning*.

Yubo Wang, Xueguang Ma, Ge Zhang, Yuansheng Ni, Abhranil Chandra, Shiguang Guo, Weiming Ren, Aaran Arulraj, Xuan He, Ziyan Jiang, and 1 others. 2024. Mmlu-pro: A more robust and challenging multi-task language understanding benchmark. In

The Thirty-eight Conference on Neural Information Processing Systems Datasets and Benchmarks Track.

Jason Wei and Kai Zou. 2019. Eda: Easy data augmentation techniques for boosting performance on text classification tasks. *arXiv preprint arXiv:1901.11196*.

Juncheng Wu, Wenlong Deng, Xingxuan Li, Sheng Liu, Taomian Mi, Yifan Peng, Ziyang Xu, Yi Liu, Hyunjin Cho, Chang-In Choi, and 1 others. 2025. Medreason: Eliciting factual medical reasoning steps in llms via knowledge graphs. *arXiv preprint arXiv:2504.00993*.

Jiaxi Yang, Wenglong Deng, Benlin Liu, Yangsibo Huang, James Zou, and Xiaoxiao Li. 2025. Gmvaluator: Similarity-based data valuation for generative models. *International Conference on Learning Representations*.

Zhengyuan Yang, Linjie Li, Kevin Lin, Jianfeng Wang, Chung-Ching Lin, Zicheng Liu, and Lijuan Wang. 2023. The dawn of lmms: Preliminary explorations with gpt-4v (ision). *arXiv preprint arXiv:2309.17421*, 9(1):1.

Xiang Yue, Yuansheng Ni, Kai Zhang, Tianyu Zheng, Ruoqi Liu, Ge Zhang, Samuel Stevens, Dongfu Jiang, Weiming Ren, Yuxuan Sun, and 1 others. 2024. Mmmu: A massive multi-discipline multimodal understanding and reasoning benchmark for expert agi. In *Proceedings of the IEEE/CVF Conference on Computer Vision and Pattern Recognition*, pages 9556–9567.

Xiaoman Zhang, Chaoyi Wu, Ziheng Zhao, Weixiong Lin, Ya Zhang, Yanfeng Wang, and Weidi Xie. 2023. Pmc-vqa: Visual instruction tuning for medical visual question answering. *arXiv preprint arXiv:2305.10415*.

Yize Zhao, Tina Behnia, Vala Vakilian, and Christos Thrampoulidis. 2024. Implicit geometry of next-token prediction: From language sparsity patterns to model representations. *arXiv preprint arXiv:2408.15417*.

Xinyu Zhou, Simin Fan, and Martin Jaggi. 2024. Hyperinf: Unleashing the hyperpower of the schulz's method for data influence estimation. *arXiv preprint arXiv:2410.05090*.

Zoheb. 2023. zoheb/sketch-scene · Datasets at Hugging Face. https://huggingface.co/datasets/zoheb/sketch-scene. [Accessed 24-09-2023].

Yuxin Zuo, Shang Qu, Yifei Li, Zhangren Chen, Xuekai Zhu, Ermo Hua, Kaiyan Zhang, Ning Ding, and Bowen Zhou. 2025. Medxpertqa: Benchmarking expert-level medical reasoning and understanding. *arXiv preprint arXiv:2501.18362*.

Contents

A More Details and Results

A.1 Additional Details

Training setting for baselines. While `For-Value` requires only a single forward pass, the influence function-based baselines `Hessian-free` and `DataInf` require fine-tuning the models to convergence. For text generation tasks, we follow the training setup in (Kwon et al., 2024), except to llama-2-13B, we use float16 weights instead of 8-bit quantization. For image-to-text generation tasks, we apply LoRA to every query and value matrix within the model's attention layers. To finetune VLMs, we use a learning rate of 2×10^{-4}, LoRA hyperparameters $r = 8$ and $\alpha = 32$, float16 model weights, a batch size of 32, and train for 20 epochs.
Efficiency details. For `For-Value`, we use a single A100 for small models. For larger 32B and 72B models in Fig. 4, inference is run on 4 A100 GPUs, while value computation is performed on a single A100. Baseline methods that require training are fine-tuned using up to 8 GPUs (for 32B models); valuation is still conducted on one A100, with 8-bit quantization applied to Qwen-32B to satisfy memory constraints. Due to their high computational cost, baselines are evaluated only on the sentence transformation task, and for 14B and 32B models we subsample 10% of the valuation data and scale the measured runtime by a factor of 10 to estimate total cost. Despite these favorable conditions, `For-Value` achieves substantially lower runtime without quantization and using fewer GPUs. For data selection experiments, all methods are evaluated on a single H100 to ensure a fair comparison.

A.2 Additional Results

Complexity Analysis. Tab. 6 compares the training, computational, and memory costs of different methods. Traditional approaches such as IF, `Hessian-free`, `HyperINF`, and `DataInf` rely on gradient traces or Hessian computations, resulting in high costs that scale poorly with model size. In contrast, `Emb` and `For-Value` are training-free and algorithm-agnostic, which significantly reduces overhead. Although `HyperINF` is the strongest baseline in terms of accuracy, its cubic complexity makes it impractical for large LLMs—requiring about 6 hours for a Qwen-32B model (Fig. 4b). Although `Emb` achieves the best runtime efficiency, its performance lags behind other methods, as demonstrated in Tab. 1 and Tab. 2. Our method, `For-Value`, maintains strong performance while remaining highly efficient. Since $|\hat{\mathcal{V}}|$ is typically small (often under 2k), `For-Value` achieves much lower computational and memory costs than baselines.
Discussion on Parallel Computing: While previous studies focus on using a single GPU for fair comparison, we would like to highlight that `For-Value` can further improve efficiency through parallel computing with a large batch size, as it only requires forward calculations. In contrast, baseline methods require computing the gradient for each individual data sample, which restricts them to a batch size of one and makes scaling up challenging.
Qualitative Demonstration. Beyond quantitative results, we present qualitative examples identified by `For-Value`. Fig. 5 shows a target valuation sample alongside its most and least influential training samples as ranked by `For-Value`. Specifically, `For-Value` successfully identifies highly relevant training points — for example, selecting samples from the same reverse order of words task for sentence transformation, or matching the same subject or artistic style in image-to-text tasks. In contrast, the least influential samples are clearly less relevant and often differ entirely in task or content from the target valuation data.
Performance of `For-Value` on different Mislabeled Ratio We evaluate the performance of `For-Value` under varying mislabeling ratios. As shown in Tab. 7, `For-Value` consistently achieves high mislabeled data detection rates, demonstrating its robustness and effectiveness across different noise levels.

A.3 Additional Details of Select Data for Finetuning

Mathematics: GSM8K As the baseline methods require LoRA, we begin with a one-epoch warmup training on Llama3-8B (Meta, 2024) using the whole training set to avoid utilizing gradients from randomly initialized LoRA modules (with a rank of $r = 32$). Next, we calculate influence scores for both the baselines and `For-Value`. To ensure consistency and performance, we also perform a one-epoch warm-up but with full-parameter finetuning on the entire dataset. Finally, we select the top 5% of data based on these influence scores to further finetune the model with learning rate $1e-5$ and batch size 64 on 4 H100 GPU for 4 epochs.
Medicine: Noise-Huatuo-Complex-CoT As the baseline methods utilize LoRA, we begin with a one-epoch training on Llama3-8B-

Method	Training Free	Algorithm Agnostic	Training Complexity	Computational Complexity	Memory Complexity
Original IF	✗	-	$O(nEd_{in}dL)$	$O(nd_{in}^2d^2L + d_{in}^3d^3L)$	$O(D^2L + nDL)$
`Hessian-free`	✗	✗	$O(nEd_{in}dL)$	$O(nd_{in}dL)$	$O(nd_{in}dL)$
`DataInf`	✗	✗	$O(nEd_{in}dL)$	$O(nd_{in}dL)$	$O(nd_{in}dL)$
`HyperINF`	✗	✗	$O(nEd_{in}dL)$	$O(nd^3L)$	$O(nd^2L)$
`Emb`	✓	✓	0	$O(nd)$	$O(nd)$
`For-Value` (ours)	✓	✓	0	$O(nd\|\hat{\mathcal{V}}\|)$	$O(nd\|\hat{\mathcal{V}}\|)$

Table 6: Comparison on complexity of the Influence Function (IF), `Hessian-free`, `DataInf`, `Emb`, and `For-Value`. Complexities are given assuming a multilayer perceptron (MLP) with L layers, each containing $d_{in} \times d$ neurons where d_{in} is input dimension and d is the output embedding dimension, trained for E epochs on n training samples. The parameter count is identical across layers ($D \in \mathbb{N}$), and the in-batch volcabulary size is $|\hat{\mathcal{V}}|$. Overall, `For-Value` achieves higher computational and memory efficiency than baseline methods.

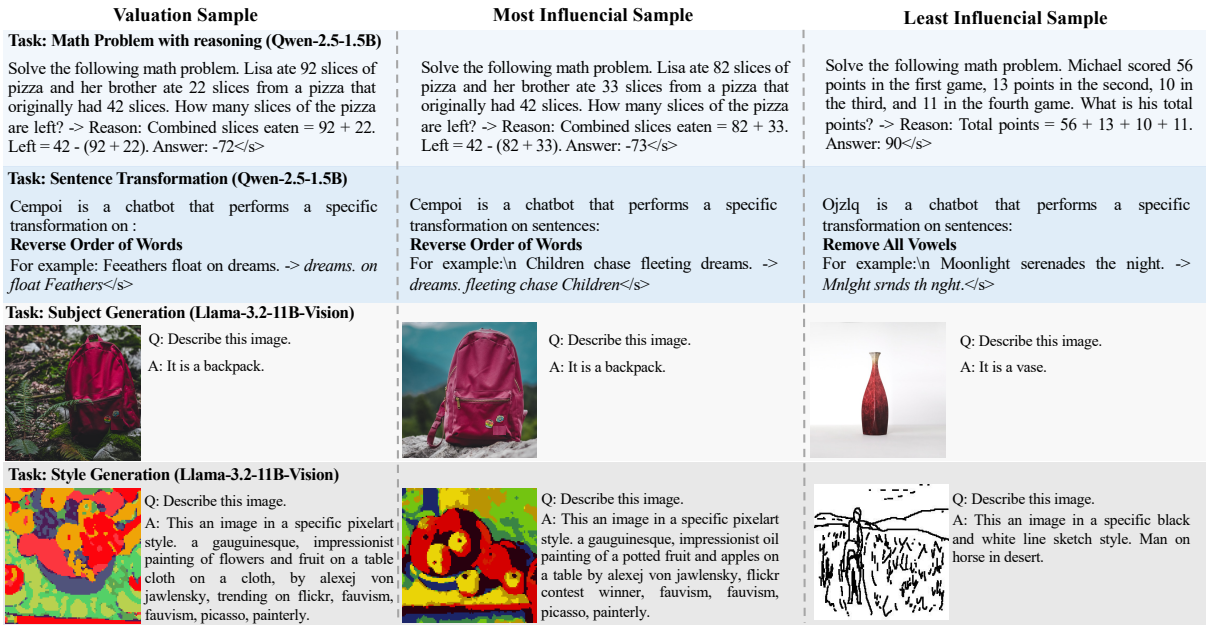

Figure 5: Qualitative examples of data influence identified by `For-Value`. For each target valuation sample (left column), the most influential (middle column) and least influential (right column) training samples are shown. `For-Value` correctly retrieves training samples that share relevant task characteristics (e.g., same reasoning type, sentence transformation rule, subject, or style) and filters out unrelated or mismatched examples.

Mislabel Ratio	Qwen2.5-VL-3B-Instruct	
	AUC ↑	Recall ↑
0.4	0.853 ± 0.048	0.972 ± 0.123
0.5	0.885 ± 0.055	0.999 ± 0.010
0.6	0.902 ± 0.046	0.952 ± 0.150

Table 7: Performance of `For-Value` on Mislabeled data detection with different noise ratio using Qwen2.5-VL-3B-Instruct.

Instruction (Meta, 2024) using the whole training set to avoid using gradients from randomly initialized LoRA modules (with a rank of $r = 16$). Next, we calculate influence scores for both the baselines and our approach. Considering the training data is noisy, we select the top 5% high value training data based on these scores and finetune the original pretrained model using full-parameter finetuning for 5 epochs, with a learning rate of 1×10^{-6}, a batch size of 16 and gradient accumulation 8 on 8 H100 GPUs. We follow (Wu et al., 2025) using greedy decoding to evaluate the model on 5 held out datasets MedQA (Jin et al., 2021), MedMCQA (Pal et al., 2022), PubMedQA (Jin et al., 2019), MMLU-Pro-Med (Wang et al., 2024), GPQA-Med (Rein et al., 2024).

Medicine: PMC-Reasoning Similarly, we start with a one-epoch warm-up on the entire training set to prevent using gradients from randomly initialized LoRA modules (with a rank of $r = 16$). Then, we compute influence scores for the baseline methods. For our method, since the pretrained model already demonstrates sufficient medical knowledge (as shown by adequate test accuracy in Table 2),

Llama-3.1-8B	Detection Accuracy
Hessian-free	48.2
HyperINF	15.1
DataInf	33.2
For-Value	84.4

Table 8: High quality data detection accuracy

we directly use the original pretrained model to assess data value. Finally, we finetune the pretrained Qwen2.5-3B-VL model (Bai et al., 2025a) with full-parameter finetuning for 3 epochs, using a learning rate of 1×10^{-5}, a batch size of 16, and gradient accumulation of 8 on 8 H100 GPUs. We evaluate the model with greedy decoding on 6 held out datasets: PMC (Zhang et al., 2023), MMMU (Yue et al., 2024), MedX-M (Zuo et al., 2025), PathVQA (He et al., 2020), SLAKE (Liu et al., 2021), VQA-Rad (Lau et al., 2018).

A.4 Additional Analysis on Select Data for Finetuning

Medicine: Noise-Huatuo-Complex-CoT. As indicated in Tab. 4, baseline methods struggle to effectively select high-quality data from noisy training datasets. This is primarily because these methods rely on assumptions of uniqueness or convergence to an optimal solution (Bae et al., 2024), which are difficult to satisfy in the presence of noisy data. To illustrate this, we evaluated the proportion of high-quality data within the top 10% of high-value data, as shown in Tab. 8. The results reveal that baseline methods generally lack the capability to accurately identify noisy data, whereas our proposed method (For-Value) achieves significantly higher accuracy in detecting clean data.

A.5 Detailed Task Description

A.5.1 LLM Influence Evaluation Tasks

Following (Kwon et al., 2024), we evaluate the performance of For-Value on three text generation tasks for large language models (LLMs) to identify influential data points:

- **Sentence Transformations:** This task requires transforming input sentences into alternative forms while preserving meaning (e.g., active to passive voice). The dataset comprises 10 distinct classes (e.g., declarative to interrogative), each with 100 examples, split into 90 training and 10 test examples per class. Data examples see Tab. 9.
- **Math Word Problems (Without Reasoning):** These problems involve direct numerical computation from textual descriptions (e.g., basic arithmetic). The dataset has 10 classes based on operation types, with 100 examples per class (90 training, 10 test). Data examples see Tab. 10.
- **Math Word Problems (With Reasoning):** These require multi-step reasoning (e.g., solving word problems involving algebra or logic). Similar to the previous task, the dataset includes 10 classes with 100 examples each (90 training, 10). Data examples see Tab. 10.

A.5.2 VLM Influence Evaluation Tasks

For VLMs, we adapt text-to-image generation tasks from (Kwon et al., 2024) into image-to-text (captioning) tasks to evaluate influence:

- **Style Generation:** This task involves generating captions for images in specific styles: cartoons (Norod78, 2023), pixel art (Jainr3, 2023), and line sketches (Zoheb, 2023). Each style dataset contains 200 training and 50 test image-text pairs, totaling 600 training and 150 test samples across three styles. Data examples see Fig. 5.
- **Subject Generation:** Using the DreamBooth dataset (Ruiz et al., 2023), this task generates captions for images of 30 distinct subjects (e.g., specific objects or animals). Each subject provides 3 training samples, with the remaining samples used for valuation. Data examples see Fig. 5.

A.5.3 Influential Data Detection Metrics

We adopt two metrics from (Kwon et al., 2024) to assess influence:

- **AUC Score:** For each test data point, we assign pseudo labels to training points (1 if the training point's label matches the test point's, 0 otherwise). We compute the Area Under the Curve (AUC) between data values (influence scores) and pseudo labels, averaging across all test points. A higher AUC indicates better identification of influential points.
- **Recall:** For each test point, we calculate the percentage of influential training points (top-ranked by influence score) that share the same class as the test point. This measures the relevance of identified influential points.

Table 9: Description of the sentence transformation task templates. We consider 10 different types of sentence transformations. For each sentence transformation, unique identifying "chatbot" names were additionally prepended to the task prompt to assist the model in training.

Sentence transformations	**Example transformation of "Sunrises herald hopeful tomorrows":**
Reverse Order of Words	tomorrows. hopeful herald Sunrises
Capitalize Every Other Letter	sUnRiSeS hErAlD hOpEfUl tOmOrRoWs.
Insert Number 1 Between Every Word	Sunrises 1herald 1hopeful 1tomorrows.
Replace Vowels with *	S*nr*s*s h*r*ld h*p*f*l t*m*rr*ws.
Double Every Consonant	SSunrriisseess hheraldd hhopefull ttomorrows.
Capitalize Every Word	Sunrises Herald Hopeful Tomorrows.
Remove All Vowels	Snrss hrld hpfl tmrrws.
Add 'ly' To End of Each Word	Sunrisesly heraldly hopefully tomorrows.ly
Remove All Consonants	uie ea oeu ooo.
Repeat Each Word Twice	Sunrises Sunrises herald herald hopeful hopeful tomorrows. tomorrows.

Table 10: Description of the math problem task templates. We consider 10 different types of math word problems.

Math Word Problems	**Template prompt question**
Remaining pizza slices	Lisa ate A slices of pizza and her brother ate B slices from a pizza that originally had C slices. How many slices of the pizza are left? Reason: Combined slices eaten = A + B. Left = C - (A + B).
Chaperones needed for trip	For every A students going on a field trip, there are B adults needed as chaperones. If C students are attending, how many adults are needed? Reason: Adults needed = (B * C) // A.
Total number after purchase	In an aquarium, there are A sharks and B dolphins. If they bought C more sharks, how many sharks would be there in total? Reason: Total sharks = A + C.
Total game points	Michael scored A points in the first game, B points in the second, C in the third, and D in the fourth game. What is his total points? Reason: Total points = A + B + C + D.
Total reading hours	Emily reads for A hours each day. How many hours does she read in total in B days? Reason: Total hours read = A * B.
Shirt cost after discount	A shirt costs A. There's a B-dollar off sale. How much does the shirt cost after the discount? Reason: Cost after discount = A - B.
Area of a garden	A rectangular garden has a length of A meters and a width of B meters. What is its area? Reason: Area = A * B.
Total savings	If Jake saves A each week, how much will he save after B weeks? Reason: Total savings = A * B.
Number of cupcake boxes	A bakery sells cupcakes in boxes of A. If they have B cupcakes, how many boxes can they fill? Reason: Boxes filled = B // A.
Interest earned	John invests A at an annual interest rate of B%. How much interest will he earn after C years? Reason: Interest = (A * B * C) // 100.

A.5.4 Mislabeled Data Detection Data & Metrics

For mislabeled detection, we transform the dataset into a visual-language question answering task with the template "What is the animal in the image? It is a [label]" with demonstration[3] in Fig. 6. We then select the first 400 images for both dogs and cats,

[3]To prevent any licensing issues, the images shown are not from the original dataset; they were personally captured for demonstration purposes.

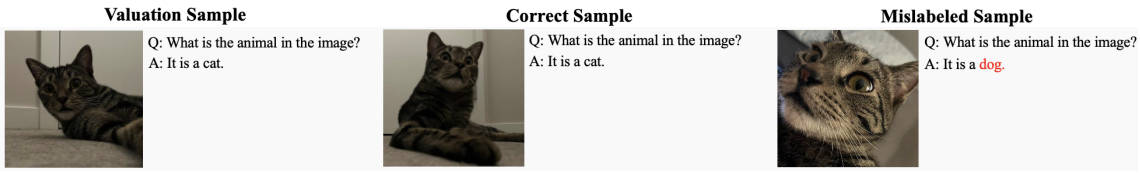

Figure 6: Description of the mislabeled data detection task. We utilize a cat versus dog classification dataset and intentionally introduce noise by randomly swapping the labels of 50% of the data.

flipping 50% of the labels to introduce noise. For valuation, we use 200 images, with each class containing 100 images. For evaluation, we also calculate the AUC and Recall but with the pseudo labels to training points being 1 if the training point's label matches the test point's and it is clean data, 0 otherwise.

A.6 Noise-Huatuo-CoT Data Example

We construct the Noise-Huatuo-Complex-CoT dataset by randomly sampling 5,000 examples without replacement and following (Wei and Zou, 2019) to inject noise into 40% of them through random insertion or deletion of irrelevant words, as illustrated in Fig. 7.

A.6.1 Baseline Checkpoints Selection

For baseline methods, we select the model checkpoint with the highest test AUC, as influence function-based methods exhibit significant performance variability across training checkpoints. Notably, this variability does not correlate with validation loss, posing challenges for practical deployment. We compare `For-Value` against these baselines to ensure robust evaluation.

A.6.2 Dataset Statistics

We present dataset statistics in Tab. 11

A.7 License Clarification

The Dreambooth images have been either taken by the authors of the paper or obtained from Unsplash[4]. The file located at this link[5] includes a list of all reference links to the images on Unsplash, along with the photographers' attributions and the image licenses. The sketch images are sourced from FS-COCO (Chowdhury et al., 2022). Data attributions and image licenses can be found in the file provided at the following link[6].

[4] https://www.unsplash.com/

[5] https://huggingface.co/datasets/google/dreambooth/blob/main/dataset/references_and_licenses.txt

[6] https://github.com/pinakinathc/fscoco

A.8 Usage of Large Language Model

In preparing this paper, we made limited use of ChatGPT to support writing and editing. Specifically, LLMs were employed for language polishing, grammar refinement, and rephrasing sentences to improve clarity and readability. Importantly, all technical content, including theoretical analysis, algorithm design, and experimental results, was conceived, implemented, and validated by the authors. LLM outputs were always critically reviewed, verified, and revised before inclusion. No LLM-generated text, figures, or tables were incorporated without careful human oversight.

Random Drop	Random Insert
Question: A nucleic acid was analyzed and found to contain 32% adenine, 18% guanine, 17% cytosine and 33deg/o thymine. The nucleic acid must be: A. Single-stranded RNA B. Single-stranded DNA C. Double-stranded RNA D. Double stranded DNA	**Question:** What physiological process in the collecting tubules is most likely to be decreased upon administration of a drug that blocks epithelial sodium channels in the cortical collecting duct?
## Alright, let's figure out what kind of nucleic acid we're with here. that's adenine, guanine, 17% cytosine, and 33% first things first, in double-stranded DNA, you'd expect adenine to pair with pair with cytosine. That means their should looking at is 32% while really close. Guanine is 18% and 17%. close. This of makes me think of double-stranded DNA because that's where see this kind of pairing. wait, not jump conclusions too quickly. Single-stranded DNA doesn't really care about matching percentages, so technically, it could have any mix of bases. be single-stranded DNA? It's possible, since there's no rule the strands. Now, out instead of at 33%. If it were RNA, we'd be seeing instead, So, it can't be neither We're definitely dealing with DNA here. Hmm, circling those matching percentages of A and T, G and really at a characteristic balance. show was a reason for such balance, which seems unlikely here without any it. considering all of this, the nucleic acid we're looking DNA. The complementary just too that seems to make the most sense given we've got. ## D. Double-stranded DNA. double-stranded Additionally, presence of thymine rather uracil rules out any RNA options.	## Thinking bar bar Alright, let's think about these epithelial sodium bar foo bar bar channels. They're bar sitting there in the foo foo apical membrane of those epithelial cells – specifically in the cortical collecting duct foo baz foo bar foo – doing the job of pulling sodium foo bar bar foo bar foo bar bar from the bar tubular fluid back foo baz into bar the bloodstream. bar Super important foo for foo baz bar sodium balance, right? So, if we throw a wrench in that foo system by blocking these channels, what happens? Hmm, yeah, sodium can't baz baz bar get reabsorbed, that's for sure. Less sodium going back into the blood – that's foo baz foo significant! Now, let's consider the water side foo of things. ... of a drug that foo bar bar blocks epithelial sodium channels in baz the cortical collecting duct is sodium reabsorption. When these channels foo foo are inhibited, sodium cannot be reabsorbed from the tubular fluid back into the bloodstream. Consequently, this disruption also affects water bar foo bar reabsorption due to the osmotic relationship between bar baz sodium baz and water, and it can alter potassium handling, although foo the primary and most immediate effect is on baz baz sodium reabsorption.

Figure 7: Examples of two types of noisy data. (Left) Random word deletion, where tokens are dropped from the reasoning, for instance, 'Thinking' is removed after ##. (Right) Random word insertion, where irrelevant tokens such as 'bar,' 'foo,' and 'baz' are injected into the reasoning. Red dashes means omitted reasoning.

Table 11: Dataset statistics for LLM and VLM tasks.

Task	Training Samples	Valuation Samples
Sentence Transformations	900 (90 × 10 classes)	100 (10 × 10 classes)
Math Word Problems (No Reasoning)	900 (90 × 10 classes)	100 (10 × 10 classes)
Math Word Problems (With Reasoning)	900 (90 × 10 classes)	100 (10 × 10 classes)
Style Generation	600 (200 × 3 styles)	150 (50 × 3 styles)
Subject Generation	90 (3 × 30 subjects)	Variable (1-3) per subject
Mislabel Detection	800 (400 × 2 subjects 50% noise)	200 (100 × 2 subjects)
GSM8K	7470	1319
Noise-Huatuo-Complex-CoT	5000 (2981 clean, 2019 noise)	5000 (clean)
PMC-Reasoning (subset)	10000	5000

B Proofs

B.1 Preliminaries

Auto-Regressive Pretrained LLMs and VLMs. We examine a pretrained large language model (LLM) or vision-language model (VLM) denoted as π_θ, where θ represents its parameters. For a given input $\boldsymbol{x}$ — which may consist of text tokens, image patches, or a combination of both — the model defines a conditional probability distribution over an output text sequence $\boldsymbol{y} = (y_1, y_2, \ldots, y_{|\boldsymbol{y}|})$, factorized as:

$$\pi_\theta(\boldsymbol{y}|\boldsymbol{x}) = \prod_{k=1}^{|\boldsymbol{y}|} \pi_\theta(y_k|\boldsymbol{x}, \boldsymbol{y}_{<k}),$$

where $\boldsymbol{y}_{<k} = (y_1, \ldots, y_{k-1})$. At each step, the model predicts the next token y_k conditioned on the input $\boldsymbol{x}$ and the prefix $\boldsymbol{y}_{<k}$. This auto-regressive structure underlies most modern LLMs and VLMs, which are used in tasks such as text generation (Wu et al., 2025), image captioning (Bai et al., 2025a), and multi-modal reasoning (Achiam et al., 2023).

Training loss of LLMs and VLMs To adapt a pretrained LLM or VLM to a specific domain or task, models are typically trained on a supervised dataset $\mathcal{D} = (\boldsymbol{x}_i, \boldsymbol{y}_i)_{i=1}^n$ of input-output pairs. Training is commonly performed using the standard teacher-forcing objective, which minimizes the negative log-likelihood of the target sequence:

$$\mathcal{L}_{\mathrm{SFT}}(\theta) = -\frac{1}{n}\sum_{i=1}^{n} \ln \pi_\theta(\boldsymbol{y}_i|\boldsymbol{x}_i) = -\frac{1}{n}\sum_{i=1}^{n}\sum_{k=1}^{|\boldsymbol{y}_i|} \ln \pi_\theta(y_{i,k}|\boldsymbol{x}_i, \boldsymbol{y}_{i,<k}).$$

This objective maximizes the likelihood that the model generates the correct output sequence conditioned on the input and the ground-truth prefix at each step. The parameters are updated using gradient descent or its variants:

$$\theta \leftarrow \theta - \eta \nabla_\theta \mathcal{L}_{\mathrm{SFT}}(\theta), \quad \text{with} \quad \theta_{t=0} = \theta_0,$$

where $\eta > 0$ is the learning rate. Teacher forcing stabilizes fine-tuning by supplying the true prefix $\boldsymbol{y}_{<k}$ during training, enabling the model to align its predictions closely with the target data distribution in the new domain.

B.2 Proof of Theorem 1

In this section, we give the detailed proof of our Theorem 1, we start by proving the following theorem:

Theorem 2 *For a data $\boldsymbol{x}_v$ and its generation $\boldsymbol{y}_v$ that await valuation, at any time $t \geq 0$ of training using a training data $(\boldsymbol{x}_i, \boldsymbol{y}_i), i \in [n]$, the training data exhibits larger value to the valuation data as the following increases:*

$$\begin{aligned}
&\sum_{k=1}^{|\boldsymbol{y}_v|}\sum_{k'=1}^{|\boldsymbol{y}_i|} \alpha_{k,k'}(t) \cdot \left\langle \mathbf{h}_{\boldsymbol{x}_v, \boldsymbol{y}_{v,<k}}(t), \mathbf{h}_{\boldsymbol{x}_i, \boldsymbol{y}_{i,<k'}}(t) \right\rangle + \\
&\sum_{k=1}^{|\boldsymbol{y}_v|} \left\langle \boldsymbol{w}_{\boldsymbol{y}_{v,k}}(t) - \sum_{z\in\mathcal{V}} \pi_{\theta(t)}(z|\boldsymbol{x}_v) \cdot \boldsymbol{w}_z(t), (\boldsymbol{w}_{\boldsymbol{y}_{i,k}} - \sum_{z\in\mathcal{V}} \pi_{\theta(t)}(z|\boldsymbol{x}_v) \cdot \boldsymbol{w}_z(t)) \right\rangle
\end{aligned} \tag{3}$$

Proof:

$$\begin{aligned}
\frac{d}{dt} \ln \pi_{\theta(t)}(\mathbf{y}_v|\mathbf{x}_v) &= \left\langle \nabla \ln \pi_{\theta(t)}(\mathbf{y}_v|\mathbf{x}_v), \frac{d}{dt}\theta(t) \right\rangle \\
&= \left\langle \nabla \ln \pi_{\theta(t)}(\mathbf{y}_v|\mathbf{x}_v), -\eta \nabla \mathcal{L}_D(\theta) \right\rangle \\
&= \left\langle \nabla \ln \pi_{\theta(t)}(\mathbf{y}_v|\mathbf{x}_v), \eta \sum_{i=1}^{n} \nabla \ln \pi_{\theta(t)}(y_i|\mathbf{x}_i) \right\rangle
\end{aligned}$$

As per the unconstrained features Assumption, the model's trainable parameters are

$$\theta = \left(\boldsymbol{W}, \mathbf{h}_{\boldsymbol{x}_v}, \left\{ \mathbf{h}_{\boldsymbol{x}_v, \boldsymbol{y}_{v,<k}} \right\}_{k \in \{2,\ldots,|\boldsymbol{y}_v|\}}, \left\{ \mathbf{h}_{\boldsymbol{x}_i, \boldsymbol{y}_{i,<k'}} \right\}_{i \in [n], k' \in \{1,\ldots,|\boldsymbol{y}_i|\}} \right).$$

Unfolding the gradients with respect to these parameters yields:

$$\frac{d}{dt} \ln \pi_{\theta(t)}(\boldsymbol{y}_v|\boldsymbol{x}_v) = \left\langle \nabla_{\boldsymbol{W}} \ln \pi_{\theta(t)}(\boldsymbol{y}_v|\boldsymbol{x}_v), \sum_{i}^{n} \nabla_{\boldsymbol{W}} \ln \pi_{\theta(t)}(\boldsymbol{y}_i|\boldsymbol{x}_i) \right\rangle + \sum_{k=1}^{|\boldsymbol{y}_v|} \underbrace{\left\langle \nabla_{\mathbf{h}_{\boldsymbol{x}_v, \boldsymbol{y}_{v,<k}}} \ln \pi_{\theta(t)}(\boldsymbol{y}_{v,k}|\boldsymbol{x}_v, \boldsymbol{y}_{v,<k}), \sum_{i'=1}^{n_k} \nabla_{\mathbf{h}_{\boldsymbol{x}_v, \boldsymbol{y}_{v,<k}}} \ln \pi_{\theta(t)}(\boldsymbol{y}_{i',k}|\boldsymbol{y}_{v,<k}) \right\rangle}_{\text{(II) Training data have the same } (\boldsymbol{x}_v, \boldsymbol{y}_{v,<k})}. \tag{4}$$

where n_k is the number of training data whose input and prediction before token k are the same as valuation data $(\boldsymbol{x}_v, \boldsymbol{y}_{v,<k})$. Since we have

$$\nabla_{\mathbf{W}} \ln \pi_{\theta(t)}(z|\mathbf{x}) = \left(\mathbf{e}_z - \sum_{z' \in \mathcal{V}} \pi_{\theta(t)}(z'|\mathbf{x}) \cdot \mathbf{e}_{z'} \right) \mathbf{h}_{\mathbf{x}}^{\top}(t),$$
$$\nabla_{\mathbf{h}_{\mathbf{x}}} \ln \pi_{\theta(t)}(z|\mathbf{x}) = \mathbf{W}_z(t) - \sum_{z' \in \mathcal{V}} \pi_{\theta(t)}(z'|\mathbf{x}) \cdot \mathbf{W}_{z'}(t).$$

Putting this back in (4) together with a few algebra steps, yields

$$\frac{d}{dt} \ln \pi_{\theta(t)}(\boldsymbol{y}_v|\boldsymbol{x}_v) = \text{(I)} + \text{(II)} \tag{5}$$

where:

$$\text{(I)} = \sum_{k=1}^{|\boldsymbol{y}_v|} \sum_{i=1}^{n} \sum_{k'=1}^{|\boldsymbol{y}_i|} \alpha_{k,k'}(t) \cdot \left\langle \mathbf{h}_{\boldsymbol{x}_v, \boldsymbol{y}_{v,<k}}(t), \mathbf{h}_{\boldsymbol{x}_i, \boldsymbol{y}_{i,<k'}}(t) \right\rangle \tag{6}$$

$$\text{(II)} = \sum_{k=1}^{|\boldsymbol{y}_v|} \left\langle \boldsymbol{w}_{\boldsymbol{y}_{v,k}}(t) - \sum_{z \in \mathcal{V}} \pi_{\theta(t)}(z|\boldsymbol{x}_v) \cdot \boldsymbol{w}_z(t), \sum_{i'=1}^{n_k} (\boldsymbol{w}_{\boldsymbol{y}_{i',k}} - \sum_{z \in \mathcal{V}} \pi_{\theta(t)}(z|\boldsymbol{x}_v) \cdot \boldsymbol{w}_z(t)) \right\rangle \tag{7}$$

where $\alpha_{k,k'}(t) = \left\langle \mathbf{e}_{\boldsymbol{y}_{v,k}} - \pi_{\theta(t)}(\cdot|\boldsymbol{x}, \boldsymbol{y}_{v,<k}), \mathbf{e}_{\boldsymbol{y}_{i,k'}} - \pi_{\theta(t)}(\cdot|\boldsymbol{x}, \boldsymbol{y}_{i,<k'}) \right\rangle$. By taking the i-th sample, we can obtain Theorem 2. We observe the following:

(1) When the training input $\boldsymbol{x}_i$ differs from the valuation input $\boldsymbol{x}_v$, its influence on the valuation target arises solely through Term (I), which captures the contribution of the token embeddings and all network parameters except the token unembedding layer.

(2) The effect of the token unembeddings is concentrated in cases where the training and valuation data share the same input $\boldsymbol{x}$ and exhibit overlapping output predictions $\boldsymbol{y}$.

To eliminate this dependence on token unembeddings, we impose the following assumption:

Assumption 2 (Distinct Input) *The training dataset satisfies that no training input $\boldsymbol{x}_i$ is identical to the valuation input $\boldsymbol{x}_v$.*

Under the Assumption 2, the contribution from token unembeddings (Term (II)) vanishes, so that the influence of the training data on the valuation data arises entirely through the shared representation features captured in Term (I). This assumption is mild, as training inputs typically differ from valuation inputs in practice — especially in vision-language datasets, where the input images are almost always distinct. Extending this result to cases where training examples share the same input but differ in their outputs $\boldsymbol{y}$ is straightforward: the output prefix $\boldsymbol{y}_{<k}$ can be incorporated into the input $\boldsymbol{x}$, treating each unique pair $(\boldsymbol{x}, \boldsymbol{y}_{<k})$ as a distinct input, where $k-1$ indicates the point at which the outputs begin to differ. Combining Theorem 2 and Assumption 2 then yields Theorem 1.